ACS APPLIED MATERIALS & INTERFACES

Research Article

www.acsami.org

Mechanical Strain Induced Tunable Anisotropic Wetting on Buckled PDMS Silver Nanorods Arrays

Pratibha Goel,[†] Samir Kumar,[†] Jayati Sarkar,[‡] and Jitendra P. Singh*[,†]

[†]Department of Physics and [‡]Department of Chemical Engineering, Indian Institute of Technology Delhi, Hauz Khas, New Delhi 110016, India

Supporting Information

ABSTRACT: We report the fabrication of anisotropic superhydrophobic surface with dual-scale roughness by the deposition of silver nanorods arrays on prestretched poly(dimethylsiloxane) (PDMS) using oblique angle deposition and subsequent release of strain after the deposition, which resulted in the formation of microbuckles/wrinkles. The amplitude and periodicity of the wrinkles were tuned by varying the prestretching mechanical strain (ε) applied to the PDMS film from 0 to 30% prior to Ag nanorods deposition. The peaks and valleys in the surface topography of Ag nanorods arrays covered PDMS films lead to anisotropic wetting by water droplet. The droplet is free to move along the direction parallel to the wrinkles, but the droplet moving perpendicular to the wrinkles confront energy barrier leading to wetting anisotropy. The anisotropic wettability was tuned from 22 to 37° for 10−30% prestretched PDMS film. The dual scale roughness (nanorods on micro wrinkles) was found to be responsible for the superhydrophobicity (contact angle ∼155°) of the sample prepared for 30% prestretched PDMS film in perpendicular direction. The wetting behavior of the Ag nanorods PDMS film surface was reversibly tuned by applying the mechanical strain, which induces the change in the microscale roughness determined by amplitude (A) and periodicity (λ) of the buckles. Most interestingly, the water droplet also displayed the anisotropy in the roll-off angle. The effect of different A and λ on anisotropic wettability of Ag nanorods arrays/PDMS film was also demonstrated by lattice Boltzmann (LB) modeling. These findings may produce a promising way of controlling the direction of liquid flow such as in microfluidic devices and transportation of the microliter water droplets in a preset direction.

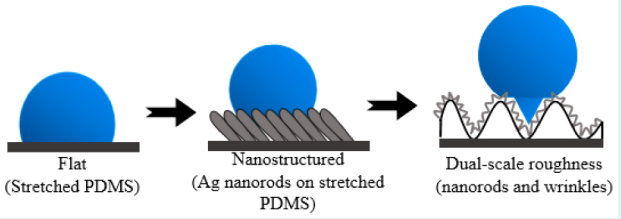

KEYWORDS: *oblique angle deposition, superhydrophobic, silver nanorods, PDMS, anisotropic wetting*

INTRODUCTION

Smart surfaces with controllable transitions of the surface wettability under external stimuli is recently been a topic of great interest because of their special applications in microfluidics, self-cleaning, biomedical engineering, and robotics.[1−6] Many researchers have used external stimuli such as electric field,[7,8] temperature,[9,10] pH value,[11] UV light,[12,13] or combination of two or more of the above stimuli[14] to control the wettability of the smart surfaces. For example, Xia et al. have reported dual-responsive surface that can switch between superhydrophilic and superhydrophobic states by varying the temperature and/or pH value.[9] In an another research Lim et al. have demonstrated the reversible tunable wettability of the functional nanoporous multilayer film under ultraviolet (UV) irradiation.[15] PDMS surface with grooves have been fabricated by photolithography and soft lithography by some researchers.[16,17] It was found that with the increase of mechanical strain the primary anisotropic wetting of the surface turned into isotropic or a larger degree of anisotropy dependent upon the stretching direction, perpendicular or parallel to grooves, respectively. For practical applications, especially biological species should be affected under rigorous conditions such as UV irradiation, electric field and temperature change. Therefore, the search of mild stimuli for controlled surface wetting is necessary. Mechanical strain is a simple, facile, safe, biocompatible and environmentally friendly method to tune the surface wettability.

Wu and researchers have reported a curvature driven in situ switching between pinned and roll-down superhydrophobic states.[18] They prepared a poly(dimethylsiloxane) (PDMS) surface with a regular array of pillars, which exhibit curvature dependent contact angle, adhesion force and sliding angle. Some research efforts aim to design surfaces that support movement of liquid in single direction for guided liquid flow for their potential applications in microfluidics, biomedical devices, and self-cleaning.[19,20] For example, researchers have fabricated anisotropic microwrinkled surface with sinusoidal profile by using ultraviolet-ozone treated PDMS elastomer to study the anisotropic wetting.[21] There are various reports on the fabrication of a stretchable, adhesion-tunable dry adhesive by differnt methods with a surface morphology consisting of a nanopillar array on a wrinkled PDMS film.[22−24] Lin et al. have fabricated superhydrophobic surface with dual-scale roughness by coating silica nanoparticles on micro wrinkled PDMS.[25]

Received: September 27, 2014
Accepted: April 6, 2015
Published: April 6, 2015

DOI: 10.1021/acsami.5b01530
ACS Appl. Mater. Interfaces 2015, 7, 8419−8426

They demonstrated that the anisotropic wetting over such surface can be controlled by mechanical strain.

In this work, we report a new method for the fabrication of dual scale roughened surface. The dual-scale roughness was mechanically controlled to tune the anisotropic wettability and to achieve superhydrophobic state. The anisotropic wetting behavior of Ag nanorods arrays on PDMS film surface as a function of the mechanical strain was also studied by using lattice Boltzmann (LB) modeling.

EXPERIMENTAL SECTION

PDMS Substrate Preparation. The PDMS substrate (~1 mm thickness) was prepared by mixing a prepolymer (Sylgard 184, Dow Corning) with a curing agent in a 10:1 ratio at room temperature. The mixture was then poured on ultrasonically acetone cleaned Si wafer and was cured at 85 °C for 20 min.

Dual-Scale Roughness Generation. The route followed for the fabrication of dual-scale roughened surface is schematically shown in Figure 1. The PDMS film was mounted on a custom-designed strain

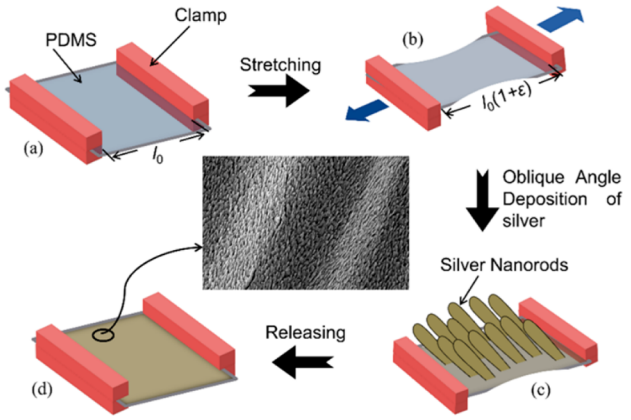

Figure 1. Schematic illustration of the fabrication of PDMS film with dual-scale roughness. (a) Clamping of PDMS film, (b) stretching the PDMS film to a designated initial strain value, (c) growth of Ag nanorods over prestretched PDMS film, and (d) releasing strain of the sample resulted into the formation of dual scale roughness as shown in magnified image.

stage to stretch uniaxially to different ratios (ε, defined as the ratio of increase in the film length (Δl) over its original length (l)). Silver films were grown over prestretched PDMS substrates by thermal evaporation of silver powder (99.9%) using oblique angle deposition (OAD) method.[26−32] For silver nanorods formation, the stretched PDMS were inclined in such a way that the substrate normal made a very high angle (α = 85°) with the direction of incident vapor flux. During the initial growth of the films, the impinging atoms form isolated nucleation centers which cast shadow for the arriving vapor flux. The nucleated islands act as shadowing centers and hence the larger nucleation centers will receive more impinging atoms as compared to the smaller ones resulting into the larger islands to grow. The competition between limited adatom surface mobility and shadowing effect results in the evolution of the columnar structure with the growth of Ag nanorods in the direction of the incident vapor flux. During deposition the substrates were kept at room temperature. The pressure of the deposition chamber was better than 2×10^{-6} Torr and the deposition rate was 14.6 Å s^{-1}. After deposition the sample was taken out from the chamber and the strain was released slowly. The microscale roughness was resulted from the internal buckling of the PDMS elastomer film and the nanoscale roughness was generated by obliquely deposited silver nanorods resulting into the dual-scale roughness as shown in the magnified image of Figure 1d.

Sample Characterization. Film morphology and structural analysis were performed using scanning electron microscope (SEM, ZEISS EVO 50). To confirm the elemental composition of the buckled PDMS/Ag nanorods arrays over an area, elemental mapping and spectra were recorded using Energy-dispersive X-ray Spectroscopy (EDX) equipped with SEM. For static contact angle measurements High performance liquid chromatography (HPLC) deionized (DI) water droplets (~5 μL) with a typical resistivity value of 18.2 MΩ cm at 25 °C were deposited on the sample surfaces. The volume of the water droplet was varied between approximately 0.5 to 20 μL for the dynamic measurement. The image of the droplet on sample was captured using CMOS camera equipped with a magnifying lens at an ambient temperature. The CA of the droplet was measured using the ImageJ software (National Institute of Health, USA). The surface topography of the samples was imaged with an atomic force microscopy (AFM) (Dimension Icon model, Bruker) in tapping mode.

RESULTS AND DISCUSSION

Morphology Characterization of the Buckled Ag Nanorod Arrays/PDMS Film. Figure 2 shows the SEM

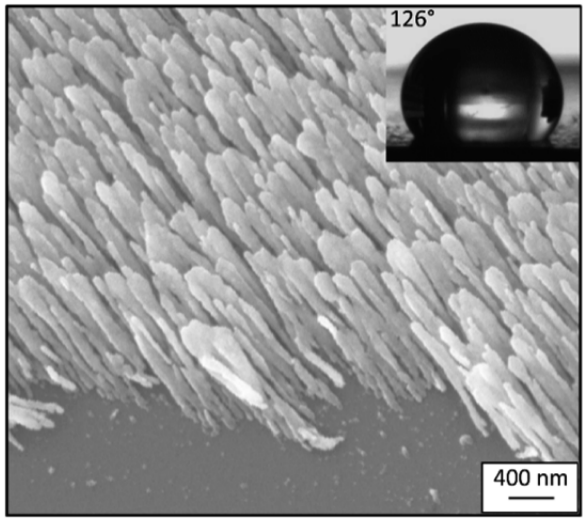

Figure 2. SEM image of the Ag nanorods arrays grown over PDMS film. The image of static water droplet (5 μL) on Ag nanorods arrays/PDMS film is shown in the inset.

micrograph of Ag nanorods arrays deposited on the unstretched PDMS film substrate. The nanorods length was about 1 μm and diameter of about 100 nm with an average internanorod separation of 130 nm. It can be clearly observed that without stretching, the primary surface consisting of nanoscale roughness due to Ag nanorods showed an isotropic wetting with a contact angle (CA) value of 126.2 ± 2.6°. The Ag nanorods deposited over prestretched elastomeric PDMS films subjected to initial mechanical strain (ε), upon releasing the strain, periodic wrinkles were formed to minimize the strain energy. The applied strain was greater than the critical strain (ε_c) value which is 10% in the present case. The formation and evolution of the wrinkles for various strain values (ε = 10 to 30%) are shown in SEM micrographs in Figure 3. The periodicity (λ) and the amplitude (A) of these wrinkles were simply tuned by varying the strain values (ε). The periodicity (λ) for the wrinkled Ag nanorods arrays on PDMS is found to be varied from 6.0 to 3.5 μm for ε varying from 10 to 30%, respectively (Figure 3a−c). The λ value of the wrinkles was calculated from the low magnification SEM (Figure S1 in the Supporting Information). The average distance between five pairs of two consecutive wrinkles was considered. There is a

DOI: 10.1021/acsami.5b01530
ACS Appl. Mater. Interfaces 2015, 7, 8419−8426

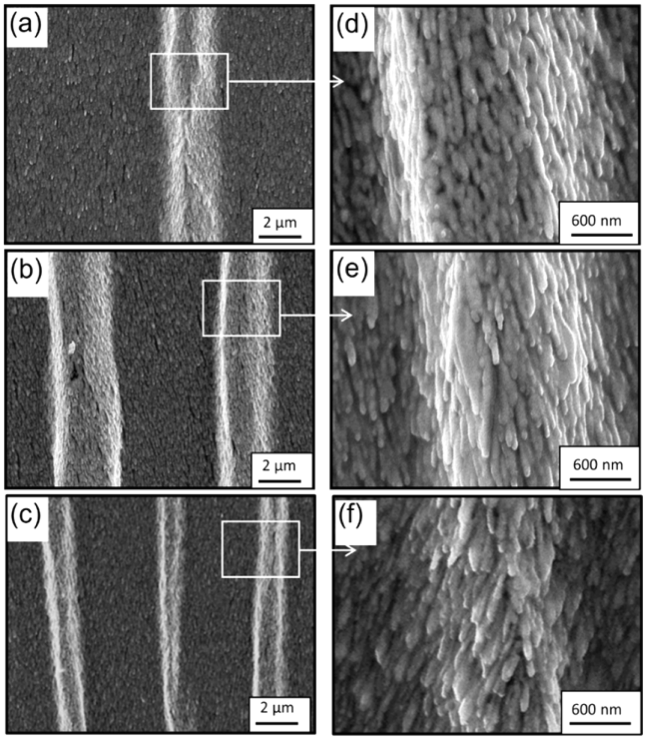

Figure 3. Effect of mechanical strain (ε) on Ag nanorods/PDMS film morphology for ε value of (a) 10, (b) 20, and (c) 30%. (d–f) Higher-magnification SEM images of the corresponding surfaces.

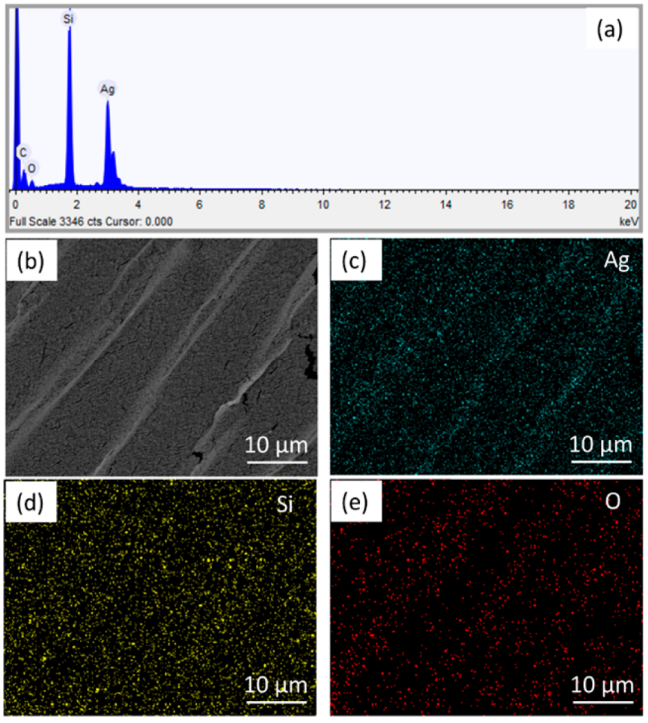

Figure 4. (a) EDX spectra, (b) SEM image of Ag nanorods samples on 30% prestretched PDMS substrate, and (c–e) elemental mappings of Ag (blue), Si (yellow), and O (red).

variation in λ value across the sample, because of the nonuniform distribution of the compressive strain. The magnified view of the corresponding wrinkled Ag nanorods arrays on PDMS are shown in Figure 3d–f. The SEM micrographs clearly show that the final sample consists of dual-scale roughness due to micrometer-sized wrinkles of PDMS and nanoscale roughness of Ag nanorods. The typical A for the dual scale roughened PDMS film obtained from AFM image (Supporting Information, Figure S2) found to be varied from 0.3 to 2.1 μm for varying ε values from 10 to 30%, respectively. Figure 4a shows the EDX spectra of the Ag nanorods buckled PDMS film prepared under 30% pre stretching. From EDX characterization results, major elemental peaks of C, O, Si, and Ag were observed. The C, O, and Si peaks originate from the polymer PDMS. The Ag peak arises from the Ag nanorods deposited over PDMS. In order to address the composition variation, we have carried out the elemental mapping during EDX (Figure 4b–e). The elemental map shows the presence of buckles and Ag over PDMS substrate.

According to the previous studies,[33,34] the wrinkle wavelength (λ_0) and amplitude (A_0) are given by

$$\lambda_0 = 2\pi h_f \left(\frac{\bar{E}_f}{3\bar{E}_S}\right)^{1/3} \tag{1}$$

and

$$A_0 = h_f \left(\frac{\varepsilon}{\varepsilon_c} - 1\right)^{1/2} \tag{2}$$

where $\bar{E} = E/(1-\nu^2)$. E, h, ν, and ε are the elastic modulus, film thickness, Poisson's ratio, and applied strain, where subscripts f and s refer to the film and the substrate, respectively. The critical strain (ε_c) must be applied for wrinkles formation and is given by[35]

$$\varepsilon_c = -\frac{1}{4}\left(\frac{3\bar{E}_s}{\bar{E}_f}\right)^{2/3} \tag{3}$$

Equation 1 shows that the wrinkle wavelength (λ) increases when the film thickness or the difference between the elastic moduli of the film and substrate increases. Because of the linear stress–strain behavior used in the derivation of eqs 1 and 2, these results can be applied to the buckling process. However, in this model, the wrinkle wavelength (λ) is independent of the prestrain (ε).

The presence of the nanostructured Ag film over PDMS results into the nonlinearity in stress–strain response. So Jiang et al.[36] updated the model, taking account of the influence of the prestrain (ε) and nonlinearity strain–displacement relation by neo-Hookean constitutive law as

$$\lambda = \frac{\lambda_0}{(1+\varepsilon)(1+\xi)^{1/3}} \tag{4}$$

$$A = \frac{A_0}{(1+\varepsilon)^{1/2}(1+\xi)^{1/3}} \tag{5}$$

where λ_0 is the wavelength in eq 1 and $\xi = 5\varepsilon(1+\varepsilon)/32$. By using the values of the parameters E_s = 1.8 MPa, E_f = 83 GPa, ν_s = 0.48, ν_f = 0.37, h_f = 0.496 μm, and ε = 0.3 ,the value of λ comes out to be 55.2 μm. The experimentally observed λ and A values are smaller than the analytical prediction. The finite deformation model proposed by Jiang et al.' which was validated for the system consisting of single-crystal silicon ribbon bonded to PDMS substrate, cannot completely predict the buckling topology of metal nanostructure/PDMS bilayer system. It is mainly because the Young's modulus of the PDMS

DOI: 10.1021/acsami.5b01530
ACS Appl. Mater. Interfaces 2015, 7, 8419–8426

film gets modified because of heating of the PDMS film during the thermal deposition of Ag film.[37,38] Second, the porosity of the Ag nanostructured film on the PDMS substrate may result into the surface layer of different elastic modulus.[39] The surface effect on wrinkling explain the deviation in experimentally observed λ and A values from the theoretically predicted values.[40]

Wetting Behavior of Buckled Ag Nanorod Arrays/PDMS film. Because of the underlying wrinkled pattern, the global shape of the water droplet did not remain circular as it appeared on the planar surface. Figure 5 shows the schematic

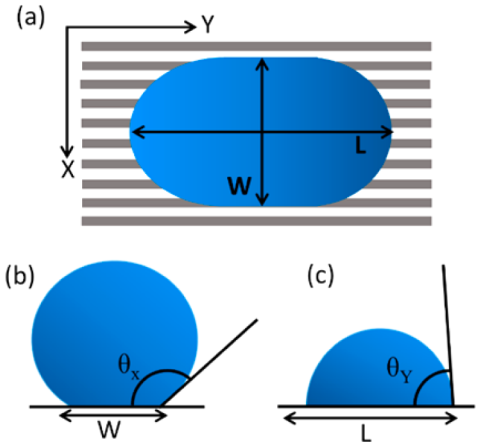

Figure 5. (a) Schematic top view of anisotropic water droplet baseline on microwrinkled surface. Contact angle profiles of (b) θ_x ($\theta_\perp$) and (c) θ_y ($\theta_\parallel$).

for an anisotropic wetting of a dual scale roughened surface. For the anisotropic wettability study, x- and y-directions are defined as the directions for two different contact angles: perpendicular ($\theta_\perp$, when the CA was measured parallel to the grooves and the contact line was perpendicular to the grooves) and parallel ($\theta_\parallel$, when the contact angle was measured perpendicular to the grooves and the contact line was parallel to the grooves). The degree of wetting anisotropy is defined as $\Delta\theta = \theta_\perp - \theta_\parallel$. The results presented in Figure 6a shows the equilibrium static water contact angle measured along perpendicular ($\theta_\perp$) and parallel ($\theta_\parallel$) to the directions of grooves (these two configurations are illustrated in Figure 5). As the strain was raised stepwise from 0 to 30%, $\theta_\perp$ increases linearly with an increase in the strain value, whereas $\theta_\parallel$ increase slightly. The anisotropy in the surface topography plays a dominant role in developing anisotropic wetting behavior at the liquid–solid interface. In an interesting study, Li and co-workers have shown the anisotropic wettability due to the pinning effect on the grating patterns.[41] The origin of the wetting anisotropy was assigned to the pinning of water droplet by the wrinkled pattern. The pinning effect imposes energy barrier which hinders the movement of the three phase contact line in the perpendicular direction other than parallel direction, resulting in higher value of $\theta_\perp$ than $\theta_\parallel$. According to the Wenzel and Cassie–Baxter models, the static contact angle varies with respect to the change in roughness of the surface. The anisotropic property of the water droplet on wrinkled PDMS/Ag nanorods arrays can be explained through these two models. In the created wrinkle pattern, water penetrates inside the surface resulting into the anisotropy in water droplet and hence the surface is in Wenzel state. As the Ag nanorods are hydrophobic ($\theta \geq 90°$), the penetration depth in the interstitial regions scales as p^2/R, where p is the nanorods spacing and R is the droplet radius.[42] Because the droplet radius (0.1 mm) is much larger than the ~100 nm nanorods spacing, penetration is negligible. Thus, droplet remains in the Cassie state on top of the Ag nanorods. Here the highest CA observed was $\theta_\perp$ = 154.8°, whereas $\theta_\parallel$ = 118°, resulting into the wetting anisotropy ($\Delta\theta$) of about = 37° for ε = 30%. This indicates that the dual scale roughness, i.e., the presence of micrometer scale wrinkles underneath the nanostructured rough Ag nanorods, significantly enhances the hydrophobicity of the surface in perpendicular direction. The experimental parameter such as Ag nanorods length was varied from 600 to 1300 nm simply by changing the deposition rate, which in turn controls λ and A of the wrinkles for the strained PDMS (Table S1 in the Supporting Information). The maximum anisotropy with superhydrophobicity was achieved for microwrinkled PDMS silver nanorods arrays having about 1 μm length of the Ag nanorods prepared under 30% prestretching of PDMS. The hierarchically wrinkled surface corresponding to ε = 30% exhibit superhydrophobicity, in one direction with CA value of about 155°. These results show that the superhydrophobic surfaces can be prepared just by changing the geometrical aspects of the surface without depending on the modification of chemical composition of the surface such as fluorination.

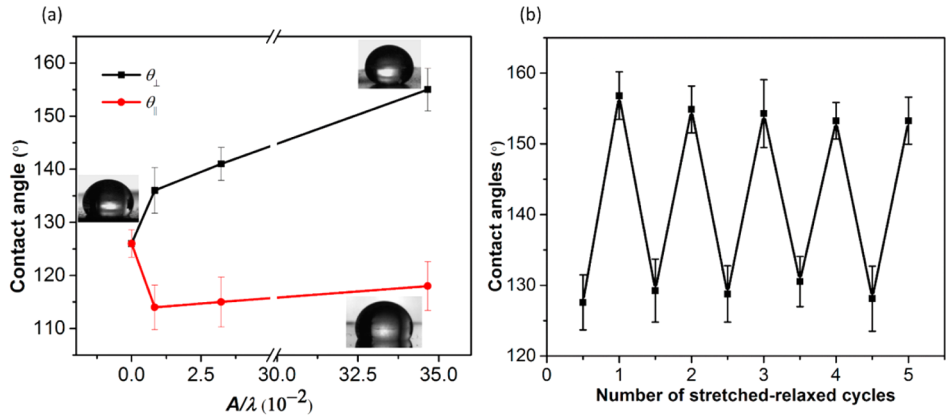

Figure 6. (a) Contact angle versus strain ε curves for different $\theta_\perp$ and $\theta_\parallel$. (b) Evolution of the contact angle for 30% prestretched PDMS sample during consecutive stretched-relaxed cycles.

DOI: 10.1021/acsami.5b01530
ACS Appl. Mater. Interfaces 2015, 7, 8419–8426

Reversibility and Repeatability of Tunable Wetting by Mechanical Strain. Due to the excellent elastic recovery of the PDMS films, multiple cycles of elongation and relaxation were studied to satisfy the demands for the practical applications. The variation in the surface properties was followed by the CA measurements. The prestretched PDMS sample with 30% strain value was switched back and forth between stretched and relaxed states and the corresponding CA ($\theta_{\perp}$) was measured throughout the process (Figure 6b). The $\theta_{\perp}$ was first observed to increase from 126.2 to 154.8° from stretched to relaxed cycle and then it decreases from 154.8 to 127.5° for relaxed to stretched cycle. The stretching of the sample to the initial strain value of 30% flattened the microscale wrinkles resulting into the sample containing only nanoscale roughness due to grown Ag nanorods. The Ag nanorods/PDMS film sample was cycled between relaxed and stretched states repeatedly and the CA was found to be reversibly tuned between two states. Because PDMS is mechanically and chemically stable. There is no need of any special protection to obtain the responsive reversibility.

To investigate the anisotropic mobility of the water droplet, we have measured the roll-off angles of 5 μL water droplets in the directions perpendicular (x) and parallel (y) to the wrinkles axis on the sample prepared for 30% prestretching as shown in Figure 7a. The roll-off in the parallel direction along the wrinkles was further measured in two opposite directions due to the directionality of the nanorods. The direction y represents the tilt of the sample where the flow of water droplet was along the nanorods and $-y$ is the direction where the flow of water droplet was against the orientation of the nanorods as shown in Figure 7c, d. It was observed in the direction x and $-y$ the water droplet did not roll-off for the sample tilting by 90°. But in x direction, the water droplet rolls off at around 70°. The original video is now provided in Supporting Information (Video S1). The difference in the sliding angle of the water droplet with respect to the orientation of the obliquely inclined nanorods can be explained by nanoscale asperities as discussed by Malvadkar and researchers in a previous study.[43]

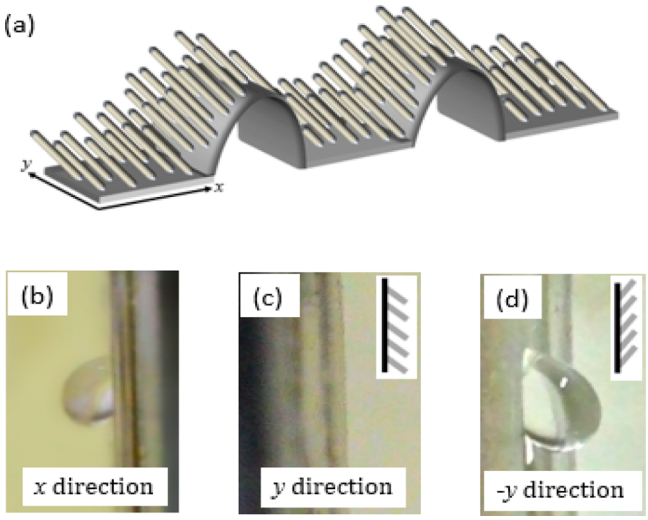

Figure 7. (a) Schematic showing the microwrinkle along with the Ag nanorods; x and y are the directions perpendicular and parallel to the wrinkle axis. (b–d) Water droplet pinning and release after tilting the samples by 90° angle in the three directions showing the anisotropic dynamic wetting behavior of the columnar films. In y direction the water droplet rolls off around 70° (see Video S1 in the Supporting Information).

Figure 8 shows the relationship between drop size and the contact angle for both advancing and receding measurement on the microwrinkled PDMS/Ag nanorods sample prepared under 30% prestretching. The sawtooth-like variation of the contact angle $\theta_{A,\perp}$ for a drop advancing perpendicular to the wrinkle axis depends upon the radius of the drop (ρ). This behavior is similar to that observed for the slip-stick of UVO treated wrinkled PDMS surface.[44] This profile can be explained by slip-stick behavior of the droplet on the wrinkled surface, which causes the contact angle to increase as the volume increases.[45] However, the three phase contact line slips when the free energy exceeds the energy of the barrier imposed by the wrinkles and the decrease in contact angle is observed. Conversely, the variation in $\theta_{A,\parallel}$ with drop radius consist of several blips resulting into decrease and then subsequent increase in the contact angle. Since simultaneous measurement of both parallel and perpendicular direction are not feasible with our system, so this behavior is under notion, but these variation in $\theta_{A,\parallel}$ may be the results of the large slip event in the perpendicular direction.

For the receding of the water droplet (Figure 8b), a different behavior is observed. For the perpendicular direction, $\theta_{R,\perp}$ decreases as the drop is pined (ρ is constant). With further decrease in the volume of the water droplet, the three phase contact line releases and decrease in ρ observed. However, $\theta_{R,\parallel}$ monotonically decreases with a decrease in the droplet volume because when the droplet recedes along the wrinkles, there is no topological energy barrier to prevent the movement of the three phase contact line.

Lattice Boltzmann (LB) Modeling of Wetting Behavior on Ag Nanorod Arrays/PDMS Film. Over the years the Johnson Dettre (JD) analytical model[46] has proved beneficial in predicting the contact angles of water droplets on ideally rough surfaces. However, because in the present study the water droplet is on a corrugated surface of the PDMS and Ag nanorod assembly having a dual scale roughness, the analytical model fails to predict the droplet wetting state as observed by experiments. The dynamics of the water droplet on the complex surface in the present paper is studied with the help of single-component multiphase LB modeling,[47,48] which is best suited for treating complex boundaries. The details of the model can be found in the Supporting Information. In simulations, the underlying corrugated substrate formed by release of the stretched PDMS is considered to be of the functional form $MAX[0,f(x) = (A - \delta)\sin(2\pi x/\lambda)]$, where $A - \delta$ is the amplitude of the buckles formed and λ is the wavelength between the buckles. The dual degree roughness brought about by the nanorods on the top of the PDMS surface is considered to be of amplitude δ in the direction of the Z-axis, of fixed lateral width w (in the direction of X-axis) and placed at a separation distance of s. The length scale ratios observed in experimental system (for example: $A/w/\delta$ or w/s) are maintained in the LB model system as well. The parameters w,s,δ are considered to have values of 1 lattice unit (lu) each. The parameter A is considered to have values of 1, 2, 3 and 4 lu in simulations and the corresponding values of considered are 8, 7, 6, and 6 lu, respectively. Initially the liquid drop is considered to have a hemispherical shape. At equilibrium, the shape of the droplet over the corrugated substrate can be visualized from Figure 9a for a 30% prestretched PDMS film. The midsection cuts parallel and perpendicular to the

DOI: 10.1021/acsami.5b01530
ACS Appl. Mater. Interfaces 2015, 7, 8419–8426

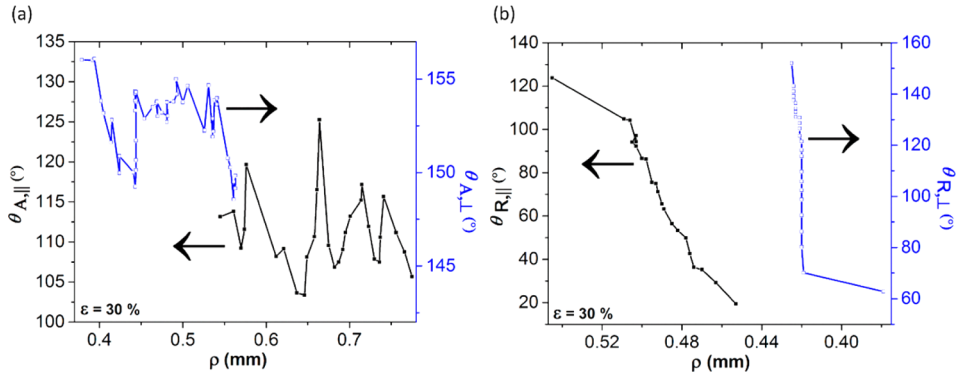

Figure 8. Variation in contact angle value for (a) advancing and (b) receding droplet on the microwrinkled PDMS/Ag nanorods arrays formed using 30% prestretching of PDMS for the drop perpendicular to the wrinkles (□) and drop parallel to the wrinkles (■).

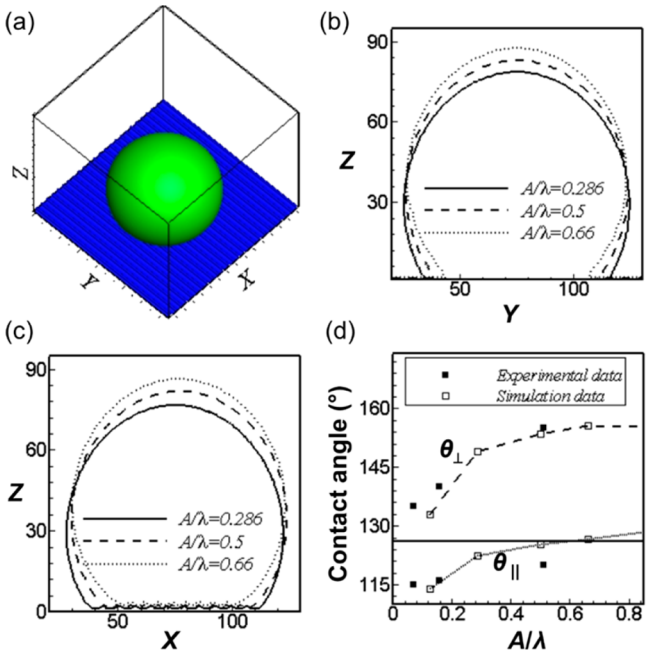

Figure 9. Simulation results showing (a) equilibrium top view of the water droplet on the Ag nanorods arrays on 30% prestretched PDMS film. The X and Y directions represent the direction perpendicular and parallel to the wrinkles. All the lengths shown are in lattice units. Mid-section cuts of the droplet in the directions (b) parallel and (c) perpendicular to the grooves. (d) Variation in contact angle with different values of A/λ, solid squares (■) show the experimental data, whereas open squares (□) show the simulation data. Solid horizontal line shows the static water contact angle value for stretched Ag nanorods/PDMS surface without wrinkles.

corrugated substrate pattern are shown in Figure 9b and Figure 9c, respectively. From Figure 9c, it was observed that the droplet follows the underlying microscopic corrugated structure and thus is in the Cassie impregnation state. It can be seen that depending on the amplitude to wavelength ratio (A/λ) of the substrate, the CA made with the substrate differs for both the cuts, where the CA is measured around $Z = A$. For the perpendicular cuts, the contact angle goes on increasing with higher amplitude ratios as shown also in earlier studies with single scaled roughness.[49] In these earlier studies, it has been found that the $\theta_{\parallel}$ for parallel cuts decreases with higher prestrain or higher A/λ ratio because the fluid needs to spread in the other direction, which leads to formation of elongated drops that lead to formation of lower contact angles. However, the $\theta_{\parallel}$ behavior exhibited in the present study is in stark contrast with those reported for single-scaled roughness. The CA here increases slightly with an increase in A/λ ratio, though the values are less than the planar contact angle value of 126°. The height of the droplets are also found to increase with increase in A/λ ratio as evident from both Figure 9b and 9c. These behaviors can be attributed to the fact that the Ag nanorods on the planar part of the PDMS act as anchors and prevent the drop from spreading in the parallel direction and this leads to overall increase in height of the droplet in both the directions. Figure 9d, shows the comprehensive plot of CA with different A/λ ratios where the straight line indicates the isotropic angle made by the droplet over the planar substrate, in the absence of any substrate roughness, and as the ratio of A/λ increases the angles formed in the two directions become anisotropic. The system becomes more hydrophobic in the direction perpendicular to the cut than in the parallel direction. The highest anisotropy in the contact angle can be observed in the vicinity of A/λ close to 0.5.

We find that the experimental data are reproduced well numerically using LB modeling. There is good agreement between the experimental and the simulation results as shown in Figure 9, for the directional contact angles as a function of A and λ of the buckles.

■ CONCLUSION

We report a new method for fabricating an elastomeric material consisting of dual-scale roughness, which exhibit mechanically tunable anisotropic wetting. The nanoscale roughness was generated by fabricating Ag nanorods arrays over prestretched PDMS film. The microscale roughness was created from the internal buckling of the PDMS elastomeric film on relaxing the strain. The Ag nanorods arrays on PDMS film with 30% prestretching was found to be superhydrophobic in one direction with the wetting anisotropy ($\Delta\theta$) of 37°. This behavior is due to the complementary micro/nano dual scale roughness presented by the surface. The wetting behavior of Ag nanorods arrays on PDMS film was simulated using LB modeling. The simulation results are consistent with the experimental results. We believe that our present study may offer new insight in designing of the rough surface for tunable wetting, which will result into the advancement of many existing technologies used in biomedical engineering and micro/nano- fluidic applications.

DOI: 10.1021/acsami.5b01530
ACS Appl. Mater. Interfaces 2015, 7, 8419−8426

■ ASSOCIATED CONTENT

Supporting Information

The SEM (Figure S1) and AFM images of the Ag nanorods arrays/PDMS film (Figure S2), Table S1 listing the anisotropy in contact angle with variation in length of Ag nanorods, the details of lattice Boltzmann (LB) modeling used for simulation, and Video S1. This material is available free of charge via the Internet at http://pubs.acs.org.

■ AUTHOR INFORMATION

Corresponding Author

*E-mail: jpsingh@physics.iitd.ac.in.

Notes

The authors declare no competing financial interest.

■ ACKNOWLEDGMENTS

P.G. gratefully acknowledges Council of Scientific and Industrial Research (CSIR), India, for the senior research fellowship. This research was funded by DST, India, Grant SR/S2/CMP-13/2010 and Nanoscale Research Facility, IIT Delhi.

■ REFERENCES

(1) Chang, B.; Shah, A.; Routa, I.; Lipsanen, H.; Zhou, Q. Surface-Tension Driven Self-Assembly of Microchips on Hydrophobic Receptor Sites with Water Using Forced Wetting. *Appl. Phys. Lett.* **2012**, *101*, 114105.

(2) Daniel, S.; Chaudhury, M. K.; Chen, J. C. Fast Drop Movements Resulting from the Phase Change on a Gradient Surface. *Science* **2001**, *291*, 633−636.

(3) He, M.; Wang, J.; Li, H.; Jin, X.; Wang, J.; Liu, B.; Song, Y. Super-Hydrophobic Film Retards Frost Formation. *Soft Matter* **2010**, *6*, 2396−2399.

(4) Jiang, C.; Wang, Q.; Wang, T. Tunable Wettability via Counterion Exchange of Polyelectrolyte Brushes Grafted on Cotton Fabric. *New J. Chem.* **2012**, *36*, 1641−1645.

(5) Xia, F.; Jiang, L. Bio-Inspired, Smart, Multiscale Interfacial Materials. *Adv. Mater.* **2008**, *20*, 2842−2858.

(6) Simao, C.; Mas-Torrent, M.; Veciana, J.; Rovira, C. Multichannel Molecular Switch with a Surface-Confined Electroactive Radical Exhibiting Tunable Wetting Properties. *Nano Lett.* **2011**, *11*, 4382−4385.

(7) Sha, M.; Niu, D.; Dou, Q.; Wu, G.; Fang, H.; Hu, J. Reversible Tuning of the Hydrophobic−hydrophilic Transition of Hydrophobic Ionic Liquids by Means of an Electric Field. *Soft Matter* **2011**, *7*, 4228−4233.

(8) Kim, T.; Lu, W.; Lim, H.; Han, A.; Qiao, Y. Electrically Controlled Hydrophobicity in a Surface Modified Nanoporous Carbon. *Appl. Phys. Lett.* **2011**, *98*, 053106.

(9) Xia, F.; Feng, L.; Wang, S.; Sun, T.; Song, W.; Jiang, W.; Jiang, L. Dual-Responsive Surfaces That Switch between Superhydrophilicity and Superhydrophobicity. *Adv. Mater.* **2006**, *18*, 432−436.

(10) He, M.; Li, H.; Wang, J.; Song, Y. Superhydrophobic Surface at Low Surface Temperature. *Appl. Phys. Lett.* **2011**, *98*, 093118.

(11) Stratakis, E.; Mateescu, A.; Barberoglou, M.; Vamvakaki, M.; Fotakis, C.; Anastasiadis, S. H. From Superhydrophobicity and Water Repellency to Superhydrophilicity: Smart Polymer-Functionalized Surfaces. *Chem. Commun.* **2010**, *46*, 4136−4138.

(12) Lim, H. S.; Kwak, D.; Lee, D. Y.; Lee, S. G.; Cho, K. UV-Driven Reversible Switching of a Roselike Vanadium Oxide Film between Superhydrophobicity and Superhydrophilicity. *J. Am. Chem. Soc.* **2007**, *129*, 4128−4129.

(13) Cui, H.; Yang, G. Z.; Sun, Y.; Wang, C. X. Reversible Ultraviolet Light-Manipulated Superhydrophobic-to-Superhydrophilic Transition on a Tubular SiC Nanostructure Film. *Appl. Phys. Lett.* **2010**, *97*, 183112.

(14) Xia, F.; Ge, H.; Hou, Y.; Sun, T.; Chen, L.; Zhang, G.; Jiang, L. Multiresponsive Surfaces Change Between Superhydrophilicity and Superhydrophobicity. *Adv. Mater.* **2007**, *19*, 2520−2524.

(15) Lim, H. S.; Han, J. T.; Kwak, D.; Jin, M.; Cho, K. Photoreversibly Switchable Superhydrophobic Surface with Erasable and Rewritable Pattern. *J. Am. Chem. Soc.* **2006**, *128*, 14458−14459.

(16) Zhao, S.; Xia, H.; Wu, D.; Lv, C.; Chen, Q.-D.; Ariga, K.; Liu, L.-Q.; Sun, H.-B. Mechanical Stretch for Tunable Wetting from Topological PDMS Film. *Soft Matter* **2013**, *9*, 4236−4240.

(17) Wu, D.; Chen, Q.-D.; Xia, H.; Jiao, J.; Xu, B.-B.; Lin, X.-F.; Xu, Y.; Sun, H.-B. A Facile Approach for Artificial Biomimetic Surfaces with Both Superhydrophobicity and Iridescence. *Soft Matter* **2010**, *6*, 263−267.

(18) Wu, D.; Wu, S.-Z.; Chen, Q.-D.; Zhang, Y.-L.; Yao, J.; Yao, X.; Niu, L.-G.; Wang, J.-N.; Jiang, L.; Sun, H.-B. Curvature-Driven Reversible in Situ Switching between Pinned and Roll-down Superhydrophobic States for Water Droplet Transportation. *Adv. Mater.* **2011**, *23*, 545−549.

(19) Bliznyuk, O.; Jansen, H. P.; Kooij, E. S.; Zandvliet, H. J. W.; Poelsema, B. Smart Design of Stripe-Patterned Gradient Surfaces to Control Droplet Motion. *Langmuir* **2011**, *27*, 11238−11245.

(20) Jokinen, V.; Leinikka, M.; Franssila, S. Microstructured Surfaces for Directional Wetting. *Adv. Mater.* **2009**, *21*, 4835−4838.

(21) Chung, J. Y.; Youngblood, J. P.; Stafford, C. M. Anisotropic Wetting on Tunable Micro-Wrinkled Surfaces. *Soft Matter* **2007**, *3*, 1163−1169.

(22) Jeong, H. E.; Kwak, M. K.; Suh, K. Y. Stretchable, Adhesion-Tunable Dry Adhesive by Surface Wrinkling. *Langmuir* **2010**, *26*, 2223−2226.

(23) Lee, E.; Zhang, M.; Cho, Y.; Cui, Y.; Van der Spiegel, J.; Engheta, N.; Yang, S. Tilted Pillars on Wrinkled Elastomers as a Reversibly Tunable Optical Window. *Adv. Mater.* **2014**, *26*, 4127−4133.

(24) Lee, S. G.; Lee, D. Y.; Lim, H. S.; Lee, D. H.; Lee, S.; Cho, K. Switchable Transparency and Wetting of Elastomeric Smart Windows. *Adv. Mater.* **2010**, *22*, 5013−5017.

(25) Lin, P.-C.; Yang, S. Mechanically Switchable Wetting on Wrinkled Elastomers with Dual-Scale Roughness. *Soft Matter* **2009**, *5*, 1011−1018.

(26) Zhao, Y.-P.; Ye, D.-X.; Wang, G.-C.; Lu, T.-M. Novel Nano-Column and Nano-Flower Arrays by Glancing Angle Deposition. *Nano Lett.* **2002**, *2*, 351−354.

(27) Singh, D. P.; Goel, P.; Singh, J. P. Revisiting the Structure Zone Model for Sculptured Silver Thin Films Deposited at Low Substrate Temperatures. *J. Appl. Phys.* **2012**, *112*, 104324.

(28) Robbie, K.; Brett, M. J.; Lakhtakia, A. Chiral Sculptured Thin Films. *Nature* **1996**, *384*, 616−616.

(29) Kumar, S.; Goel, P.; Singh, D. P.; Singh, J. P. Highly Sensitive Superhydrophobic Ag Nanorods Array Substrates for Surface Enhanced Fluorescence Studies. *Appl. Phys. Lett.* **2014**, *104*, 023107.

(30) Zhou, C. M.; Gall, D. Competitive Growth of Ta Nanopillars during Glancing Angle Deposition: Effect of Surface Diffusion. *J. Vac. Sci. Technol. A* **2007**, *25*, 312−318.

(31) Mark, A. G.; Gibbs, J. G.; Lee, T.-C.; Fischer, P. Hybrid Nanocolloids with Programmed Three-Dimensional Shape and Material Composition. *Nat. Mater.* **2013**, *12*, 802−807.

(32) Zhao, Y.; Ye, D.; Wang, G.-C.; Lu, T.-M. Designing Nanostructures by Glancing Angle Deposition. *Proc. SPIE* **2003**, *5219*, 59−73.

(33) Huang, Z. Y.; Hong, W.; Suo, Z. Nonlinear Analyses of Wrinkles in a Film Bonded to a Compliant Substrate. *J. Mech. Phys. Solids* **2005**, *53*, 2101−2118.

(34) Stafford, C. M.; Harrison, C.; Beers, K. L.; Karim, A.; Amis, E. J.; VanLandingham, M. R.; Kim, H.-C.; Volksen, W.; Miller, R. D.; Simonyi, E. E. A Buckling-Based Metrology for Measuring the Elastic Moduli of Polymeric Thin Films. *Nat. Mater.* **2004**, *3*, 545−550.

(35) Allen, H. G. *Analysis and Design of Structural Sandwich Panels*, 1st ed.; Pergamon Press: Oxford, 1969.

DOI: 10.1021/acsami.5b01530
ACS Appl. Mater. Interfaces 2015, 7, 8419−8426

(36) Jiang, H.; Khang, D.-Y.; Song, J.; Sun, Y.; Huang, Y.; Rogers, J. a. Finite Deformation Mechanics in Buckled Thin Films on Compliant Supports. *Proc. Natl. Acad. Sci. U.S.A.* **2007**, *104*, 15607−15612.
(37) Bowden, N.; Huck, W. T. S.; Paul, K. E.; Whitesides, G. M. The Controlled Formation of Ordered, Sinusoidal Structures by Plasma Oxidation of an Elastomeric Polymer. *Appl. Phys. Lett.* **1999**, *75*, 2557.
(38) Bowden, N.; Brittain, Scott; Evans, A. G.; Hutchinson, J. W.; Whitesides, G. M. Spontaneous Formation of Ordered Structures in Thin. *Nature* **1998**, *393*, 146−149.
(39) Fan, H.; Hartshorn, C.; Buchheit, T.; Tallant, D.; Assink, R.; Simpson, R.; Kissel, D. J.; Lacks, D. J.; Torquato, S.; Brinker, C. J. Modulus-Density Scaling Behaviour and Framework Architecture of Nanoporous Self-Assembled Silicas. *Nat. Mater.* **2007**, *6*, 418−423.
(40) Huang, R.; Stafford, C. M.; Vogt, B. D. Effect of Surface Properties on Wrinkling of Ultrathin Films. *J. Aerosp. Eng.* **2007**, *20*, 38−44.
(41) Li, Y.; Dai, S.; John, J.; Carter, K. R. Superhydrophobic Surfaces from Hierarchically Structured Wrinkled Polymers. *ACS Appl. Mater. Interfaces* **2013**, *5*, 11066−11073.
(42) Quéré, D. Wetting and Roughness. *Annu. Rev. Mater. Res.* **2008**, *38*, 71−99.
(43) Malvadkar, N. A.; Hancock, M. J.; Sekeroglu, K.; Dressick, W. J.; Demirel, M. C. An Engineered Anisotropic Nanofilm with Unidirectional Wetting Properties. *Nat. Mater.* **2010**, *9*, 1023−1028.
(44) Bukowsky, C.; Torres, J. M.; Vogt, B. D. Slip-Stick Wetting and Large Contact Angle Hysteresis on Wrinkled Surfaces. *J. Colloid Interface Sci.* **2011**, *354*, 825−831.
(45) Iwamatsu, M. Contact Angle Hysteresis of Cylindrical Drops on Chemically Heterogeneous Striped Surfaces. *J. Colloid Interface Sci.* **2006**, *297*, 772−777.
(46) Johnson, R. E., Jr.; Dettre, R. H. Contact Angle Hysteresis. *Adv. Chem. Ser.* **1964**, *43*, 112−135.
(47) Succi, S. *The Lattice Boltzmann Equation for Fluid Dynamics and Beyond*, 1st ed.; Oxford Science Publications: New York, 2001.
(48) Sukop, M. *Lattice Boltzmann Modeling−An Introduction for Geoscientists and Engineers*, 1st ed.; Springer: New York, 2006.
(49) Chung, J. Y.; Youngblood, J. P.; Stafford, C. M. Anisotropic Wetting on Tunable Micro-Wrinkled Surfaces. *Soft Matter* **2007**, *3*, 1163−1169.

DOI: 10.1021/acsami.5b01530
ACS Appl. Mater. Interfaces 2015, 7, 8419−8426